

NOVEL TEST RIG TO DEMONSTRATE A MULTI FUNCTIONAL FLAP MECHANISM OFFERING A 2ND DEGREE OF FREEDOM

Jan Docter¹, Hermen Pijlman¹, Dirk de Wit ², Johan Vervliet², Jordi Katarzynski¹, Royd Postma¹, Klaas-Jan Bisschop¹ & Jos Vroon¹

> ¹Royal Netherlands Aerospace Centre, The Netherlands ²Asco Industries nv/sa

Abstract

Within the consortium for "MovAbles for Next generaTion Aircrafts" (MANTA) in the frame of the Clean Sky 2 program, an innovative Multi-Functional Flap Mechanism (MFFM) is being developed, which enhances the effectiveness and expands the functionality of aircraft's control surfaces by integration of a second degree of freedom (DOF) in the flap kinematics. This innovation contributes to the Clean Sky 2 key objectives by minimizing the environmental impact of aviation and reducing CO₂ emissions by 3 to 5%.

This paper describes the test development, demonstration, virtual testing and result correlation of a simplified yet representative MFFM using a novel test rig at Royal NLR. The objective is to demonstrate that the MFFM can rotate at a speed of 60 degrees per second in retracted, take-off, and landing flap positions, under conditions of intact operation, actuator failure, and jamming scenario's. During the rotation, aerodynamic loads will be simulated using mechanical springs and masses, and wing bending will be simulated through hydraulic actuation of the wing attachments.

A separate flexible tube test demonstrates the durability of a flexible hydraulic tube attached to the MFFM. The tube must be able to withstand the aircraft's operational life under maximum operating pressure without rupturing or breaking, even under cold temperature and contaminated conditions. This paper provides the design of the tube demonstration set-up as well as the durability results.

Keywords: novel test rig, movable, virtual test model, multi-functional flap mechanism

1. Introduction & Objectives

Royal NLR [1] and ASCO [2] are core partners within a consortium named MANTA or "MovAbles for Next generaTion Aircrafts" in the frame of the Clean Sky 2 program [3]. Royal NLR is the aerospace research organization of the Netherlands and is one of its major technological institutes. As an independent non-profit organization, Royal NLR provides technical support to the aerospace sector. ASCO is a world class supplier of high lift structures, complex mechanical assemblies and major functional components with focus on the high-lift mechanisms on the leading and the trailing edge for almost all commercial aircraft platforms.

One of the key objectives of the Clean Sky 2 program is to minimize the environmental impact of aviation and reduce CO₂ emissions by 3 to 5%. MANTA contributes to this objective by increasing the effectiveness and enlarging the functionality of the control surfaces of an aircraft by a Multi-Functional Flap Mechanism (MFFM). Compared to traditional flap kinematics the aileron and high-lift functions are combined by offering a second degree of freedom (DOF) due to a variable rear link by means of an rotation actuator. Rotation actuators rotate the flap around the forward (FWD) flap lug on the carriage and translation actuators position the carriage in retracted or extending position on the track, as illustrated in Figure 1.

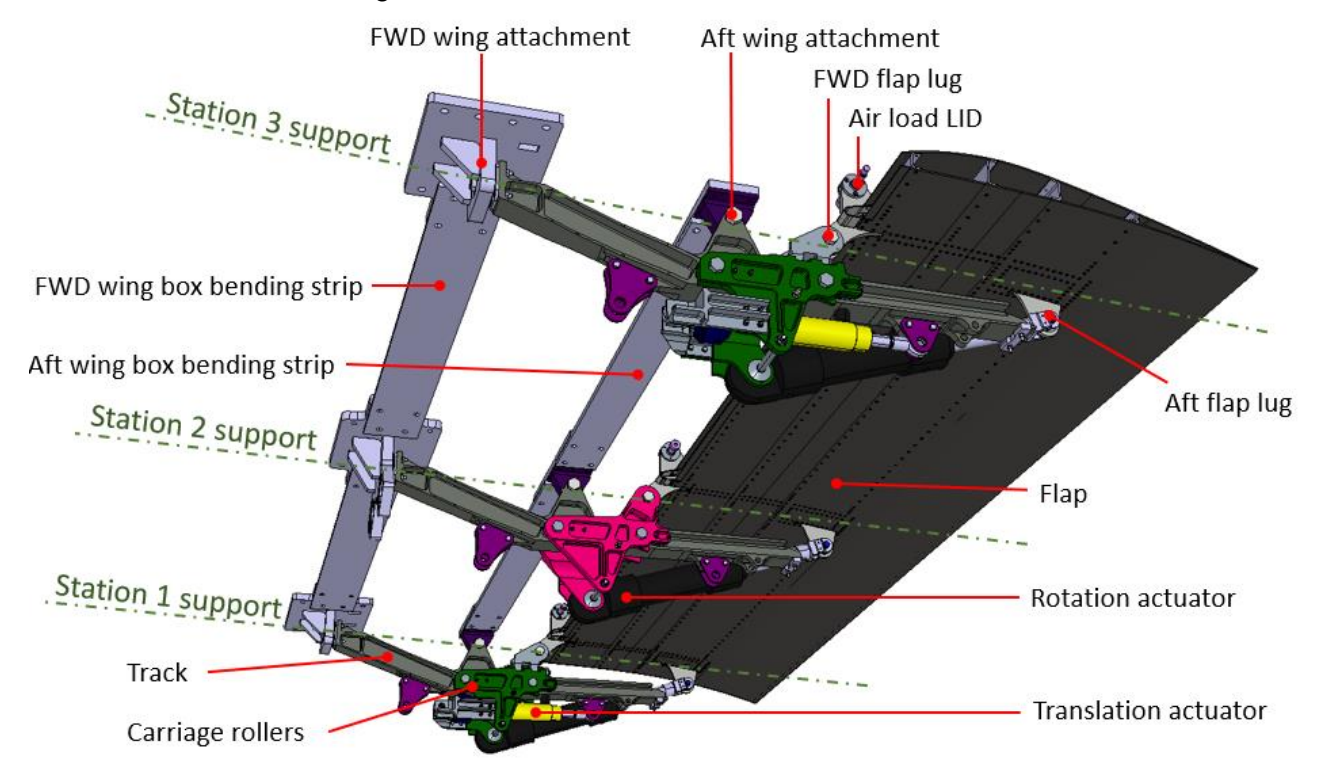


Figure 1 - Simplified but representative Multi-Functional Flap Mechanism.

This paper outlines the development, demonstration, virtual testing, and result correlation of a simplified yet representative MFFM within a novel test rig at Royal NLR, as shown in Figure 2. The primary objective is to demonstrate that the MFFM can rotate at a speed of 60 degrees per second in retracted, take-off, and landing flap positions. This demonstration considers various scenarios, including intact operation, actuator failure, and jamming cases. During the rotation, aerodynamic loads are simulated using mechanical springs and masses, while wing bending is replicated through hydraulic actuation applied to the wing attachment points.

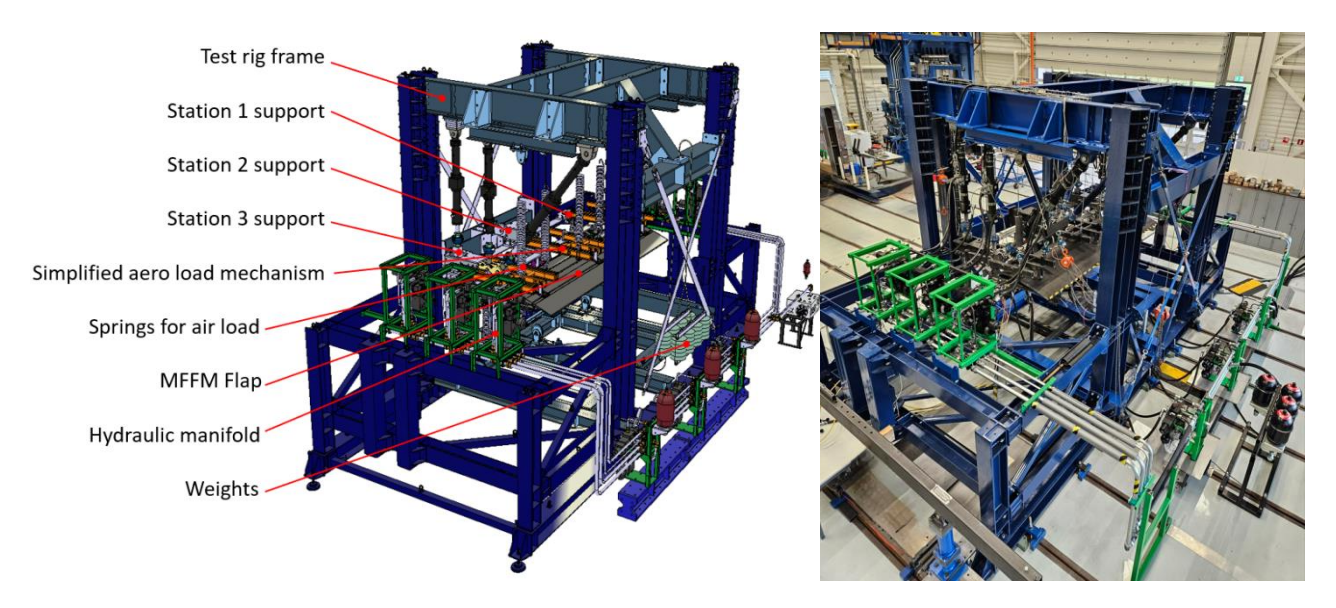


Figure 2 - Novel MANTA MFFM test rig design (left) and construction at Royal NLR (right).

To supply hydraulic pressure to the MFFM, a flexible tube is connected to the rotation actuators as illustrated in Figure 3. The tube must be able to withstand the aircraft's operational life under maximum operating pressure without rupturing or breaking, even under cold temperature and contaminated conditions. As specific section of this paper presents the design of the tube demonstration test setup as well as the durability results.

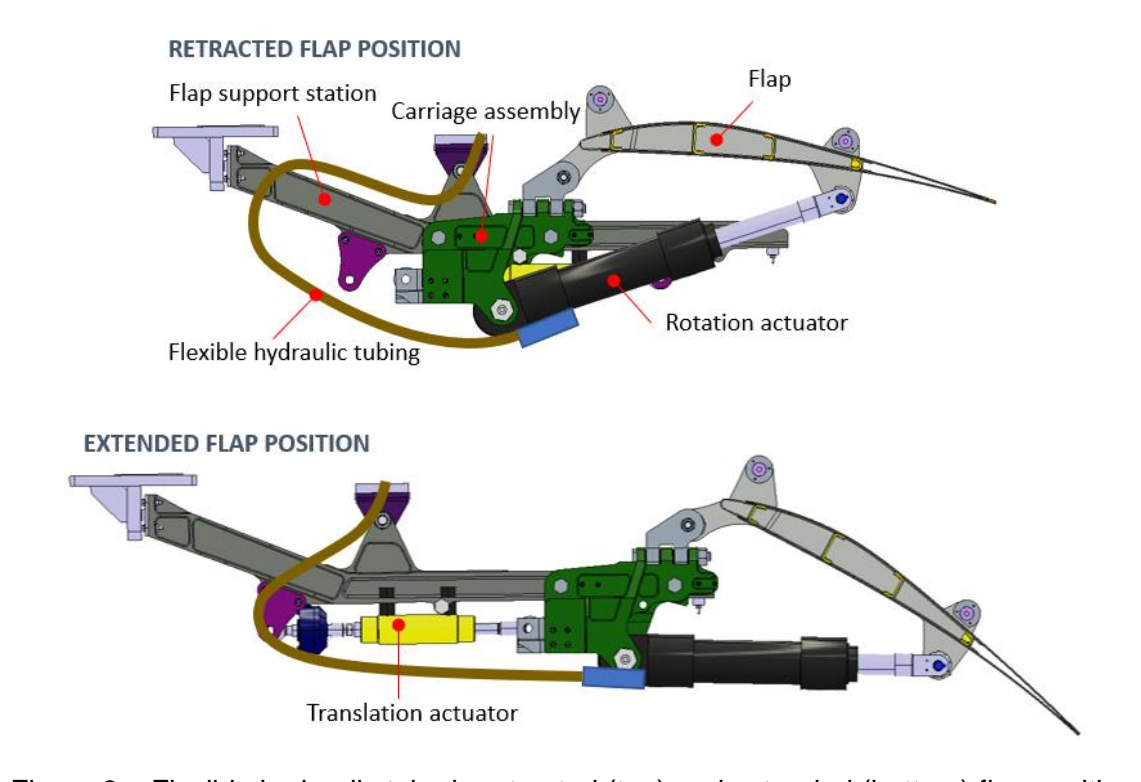


Figure 3 – Flexible hydraulic tube in retracted (top) and extended (bottom) flap position.

2. MFFM Test rig concept development

2.1 Test rig introduction

In the process of developing a functional mechanism for this novel flap kinematics, demonstration tests play a crucial role. The main challenge in designing the test rig is to show, that it is possible to operate a flap support mechanism and rotate a flap with representative stiffness and inertia properties at a speed of 60 degrees per second in retracted, take-off, and landing flap positions, considering scenarios of intact operation, actuator failure, and jamming. For this purpose a structurally complete flap and flap support mechanism, as illustrated in Figure 1, served as a starting point, interfacing with three nearly identical flap supports to the test rig. Each flap support consists of structural components with a track, carriage, carriage rollers, forward (FWD) and aft (AFT) wing attachments, and the FWD and AFT flap lugs interfaces. Each support is equipped with a rotation actuator, however, only the outboard and inboard flap supports on station 1 and station 3 are equipped with a translation actuator. The rotation actuator enables the rotation of the flap, while the translation actuator moves the flap and carriage to either the extended or retracted flap position along the track. Additionally, during the failure ultimate tests, in the event of a jamming condition, the translation actuator system will be used to introduce the ultimate load limiter setting or to keep the carriage in position when the maximum skew in the flap is reached.

In order to impose the loads and displacements on the test article for each test case, 4 main functions of the test rig are derived. Those are depicted in Figure 4 and elaborated in more detail in de following sub sections:

- 1. Static positioning of the flap on the track, for the intact retracted or extended flap position case.
- 2. Semi static wing bending application by positioning the FWD & AFT wing attachments.
- **3.** Dynamic Air load application, for simulating the flap air load moment around the FWD flap lug during flap rotation.
- **4.** Dynamic flap rotation, for demonstrating that the flap can rotate at 60°/s while being subjected to wing bending and air load in retracted and extended position on the track.

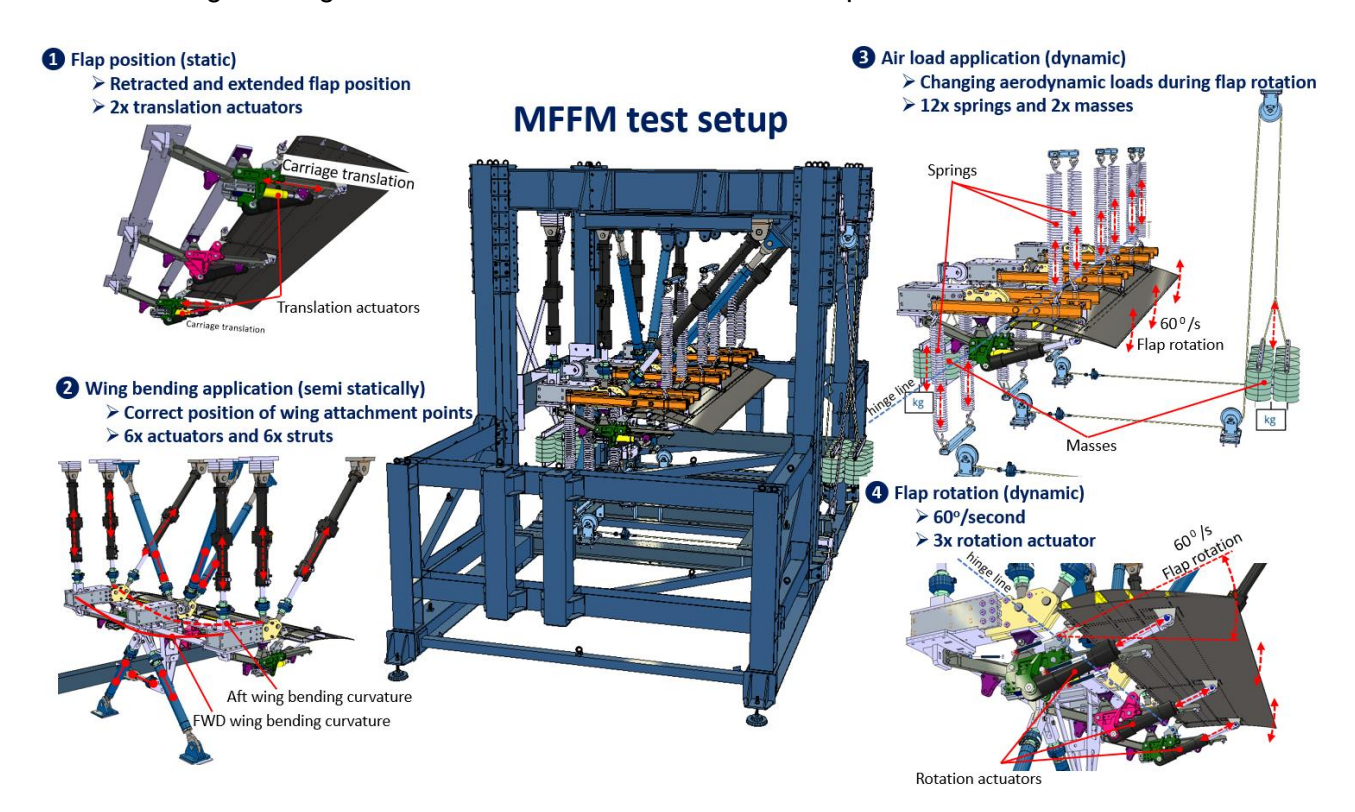


Figure 4 – MFFM test setup main functions.

The demonstration loading conditions result from the most critical intact conditions of the MFFM [3]. In addition to the standard intact tests, failure ultimate tests were performed. These failure ultimate tests are similar intact test cases but include one of the following failures;

- Disconnect of the translation actuator, where one of the translation actuators is removed from the test setup, allowing the carriage to move freely on the track.
- Disconnect of the rotation actuator, where one of the rotation actuators is removed from the test setup and the remaining rotation actuators rotate the flap.
- Jamming of carriage, where one of the carriages is jammed at its nominal position. The jamming is replicated by inserting the rigging pin through the carriage and track.

A schematic diagram of the performed demonstration tests is given in Figure 5.

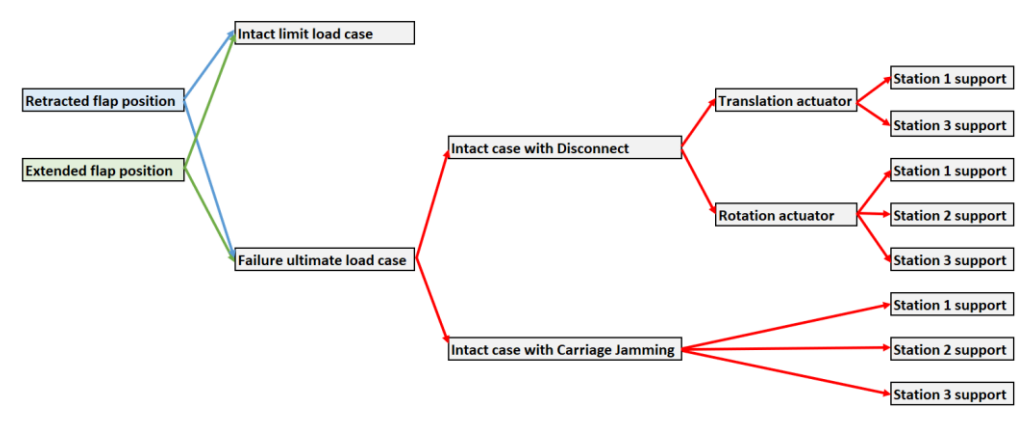


Figure 5 – Schematic diagram of the demonstration tests.

2.2 Static Positioning of the flap on the track

The translation actuator moves the carriage along the track, adjusting the flap to the desired position. As illustrated in Figure 1, only the inboard and outboard flap support stations are equipped with a translation actuator. During the MFFM demonstration test, the focus is on two positions: the retracted and extended flap positions. In the event of a failure case, the translation actuator is disconnected or the carriage support is jammed, for the latter the translation actuator is adjusted to the ultimate load limiter setting or to the maximum skew angle, whichever occurs first. For simplicity, manual control of the translation actuator using a hand pump was chosen. The loads and displacements for each translation actuator are measured.

2.3 Semi Static Wing bending application

Wing deformation impacts various requirements. The hinge line around which the flap rotates is not straight anymore due to the wing deformation. This deformation introduces a relative displacement and rotation between pairs of tracks, leading to force-fighting between the different track supports when rotating the flap body. It is essential to ensure and demonstrate seamless operational performance in terms of translation and rotation of the flap body.

The wing bending and twisting is replicated by introducing displacements with six test rig actuators at the FWD and AFT wing attachment of the two outer support stations and constraining the centre support station with six struts. A complete wing box is not considered in this test setup. The deformation of a complete wing box would have required significantly greater actuator loads for the same outcome, necessitating a stiffer and stronger test rig. The dummy wing box is built up from a FWD and AFT wing box bending strip which is bolted to each of the three stations as depicted in Figure 1. These bending strips are tailored to convert the displacements of the test rig actuators to the actual displacements of the wing interfaces and support the stations in the sideward direction.

For the MFFM demonstration test, only the correct positions at the FWD and AFT wing attachment of the three stations are of importance. The deformation of the wing box between the stations has no impact on the flap. All given Finite Element Model (FEM) displacements are relative to the FWD wing attachment at support station 1. But since it is more convenient to constrain station 2 as a fixed interface for the test rig design and testing, the wing bending displacements are translated and rotated, as illustrated in Figure 6, to maintain the same relative wing bending curvature. The advantages of fixing station 2 instead of the other stations include; no initial rotation at the fixed Aft wing attachment station, smaller actuator displacements resulting in a more compact test setup, minimized side load introduction due to changes in actuator angles while retracting and extending, and easier application of air loads with the simplified air load mechanism.

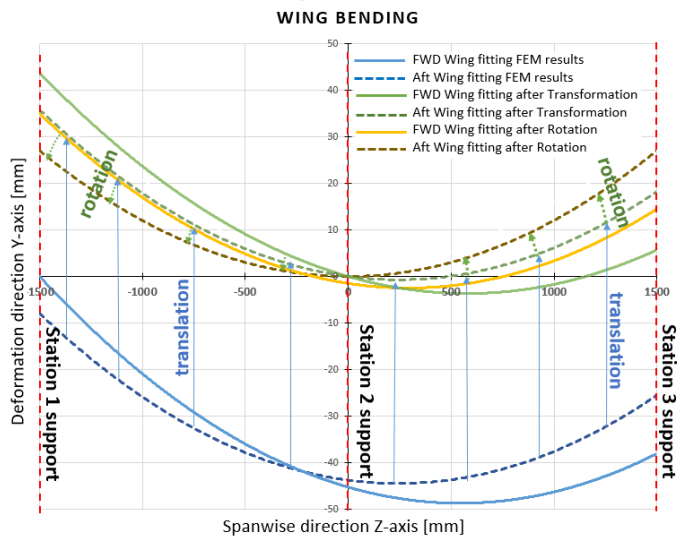


Figure 6 – Wing bending represented by (vertical) displacements on FWD & AFT wing attachments at Station 1, 2 and 3.

Since the test rig actuators are displacement controlled to apply wing bending, the deformations of the test rig frame must be accounted for. However, because the finite virtual test model showed minimal test rig deformations, it was decided that no corrections were needed, when applying the wing bending to the test structure, see Figure 7.

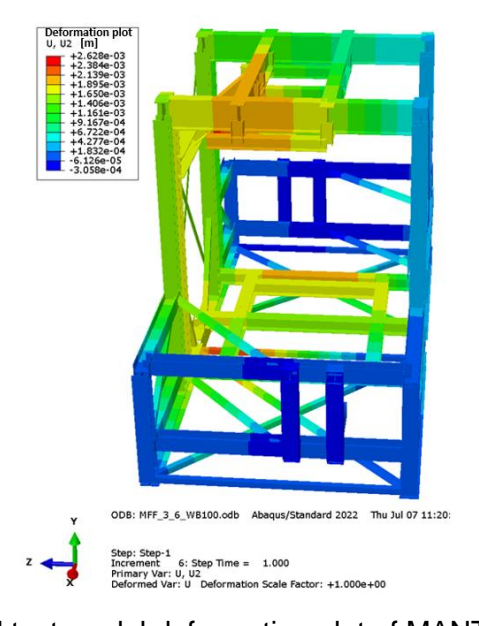


Figure 7 – Virtual test model deformation plot of MANTA MFFM test rig.

2.4 Air load application by masses & springs

In real-life aircraft applications, the aerodynamic load changes during flap rotation, and also due to the varying shape of the flap in the spanwise direction. As a result, the aerodynamic loads differ between the three stations. A simplified aero load mechanism is developed to mimic the changing aerodynamic loads, while the flap rotation, is controlled by a displacement-controlled rotation actuator. After examining the given aerodynamic FEM loads on the flap, it was observed that for nearly all load conditions, the air load either linearly increased or decreased with the flap rotation angle, except for support station 2 when the carriage is in the extended position. In this scenario, the air loads remain almost constant.

To eliminate the risk of force fighting between the three displacement-controlled rotation actuators and the aero load actuators, as well as the need for the aero load actuators to follow the rotating flap, a decision was made to apply the aerodynamic loads using a passive loading method, more specifically through the use of springs and masses. This approach ensures smoother operation and avoids conflicting forces during the demonstration tests.

The objective is to demonstrate the capability of rotating the flap body and so the work to be delivered by the rotation actuator, which is directly related to the moment around the 'FWD flap lug'. Therefore, it was decided to simplify the aero load mechanism and to mimic the moment (*Mz*) around the 'FWD flap lug', rather than the force at the 'FWD flap lug'.

A schematic sketch of the simplified aero load mechanism with pulleys, springs and masses is shown in Figure 8. The 'FWD flap lug' is attached to the carriage, and the 'AFT flap lug' is directly connected to the rotation actuator, which is also fixed to the carriage. At each flap support station, two additional lugs are mounted on top of the flap flange. These lugs are connected to the Air Load Introduction Device (Air LID). The 'FWD air lug' is directly connected to the 'Air LID', while the 'AFT air lug' is connected via a 'swing link,' as illustrated in the sketch.

The FEM predictions indicate that at certain track support stations, the moment around the 'FWD flap lug' remains constant, while at others, it increases or decreases as the flap rotates. To maintain a constant moment around the 'FWD flap lug', masses can be attached to the 'Air LID' at equal distances from the 'FWD flap lug'. The same approach can be applied to the springs, with the exception that for springs, the moment varies linearly based on the spring characteristics and the displacements caused by the flap's rotation. Pre-tensioning the spring allows for the generation of an initial moment.

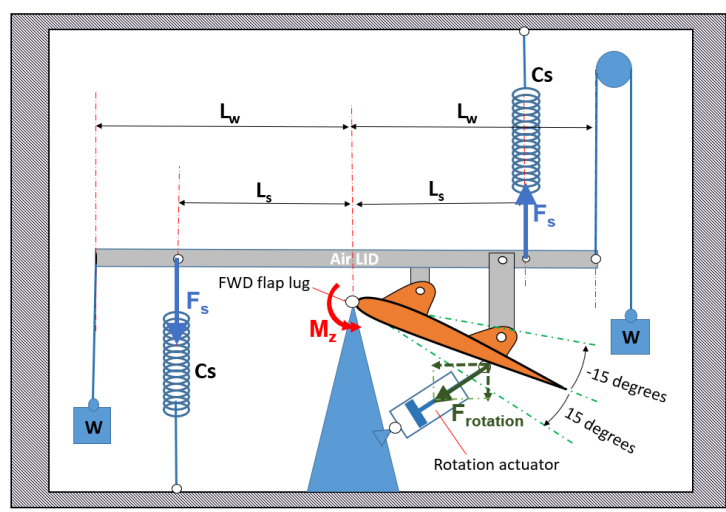


Figure 8 – Schematic sketch of the simplified aero load mechanism.

2.5 Flap rotation

Flap deployment is controlled by the three rotation actuators attached to the AFT flap lugs and the lower carriage lugs. By adding this functionality into the MFFM, the omission of high and low-speed ailerons becomes possible. The flap rotation is limited to +/-15degrees in both the retraced and extended positions, as shown in Figure 9. However the operating stroke length differs. To ensure proper flap functionality, it must be demonstrated that the flap movement achieves at least 60 degrees per second in each setting. Additionally, the rotation actuator load should match the *Mz* moment derived from the simplified aero load mechanism, as illustrated in Figure 8. This demonstration is necessary not only for the intact retracted and extended flap positions but also in the event of failure, such as when the translation actuator or rotation actuator is disconnected or a carriage support is jammed.

It's important to note that these rotation actuators are not standard test rig actuators. They were selected based on load specifications, motion requirements, operation pressure, flow rate, and available installation space.

Tailor designed load pins are used to measure the rotation actuator loads, while external LVDTs measures the displacements.

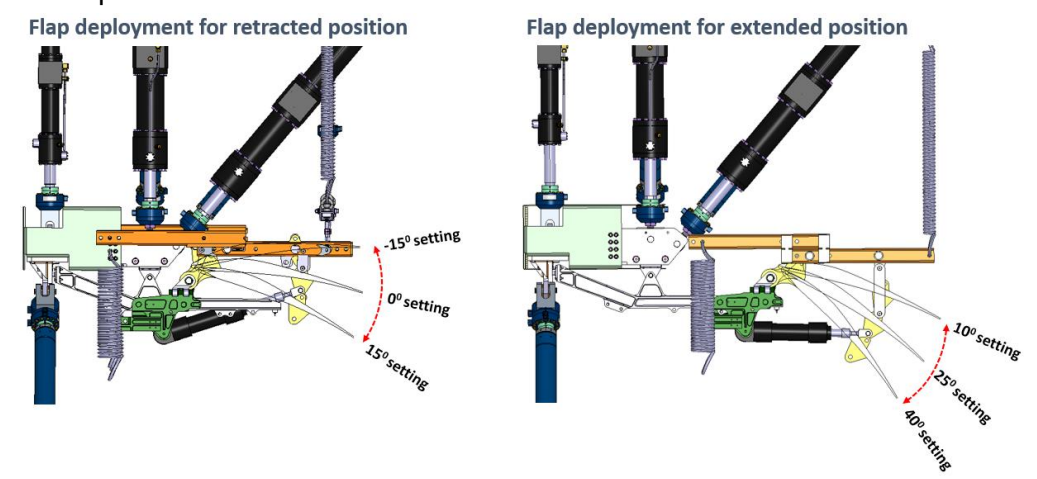


Figure 9 – Flap position and deployment angles.

2.6 Hydraulic layout

In order to define the layout of hydraulic actuators, valves, piping, manifolds and accumulators, the most severe conditions with respect to test loads and velocities are considered for the main functions of the test rig: semi static wing bending and dynamic flap rotation. The other functions are executed manually and do not affect the hydraulic layout.

For both functions the minimal actuator piston effective areas are calculated, assuming a constant available hydraulic system pressure:

$$A_i = \frac{F_{i,wc}}{p_s} \qquad i = 1 \text{ to } 9 \tag{1}$$

where

- A_i are the minimal effective actuator piston areas
- F_{i,wc} are the worst case actuator loads in the test set-up
- p_s is the system pressure (200 bar at NLR)

Subsequently the required displacement velocities are determined, considering a sinusoidal trajectory to realize a rotation speed of 60°/s:

$$\dot{s}_{i} = 0 \qquad i = 1 \text{ to } 6$$

$$\dot{s}_{i} = \dot{\alpha} \cdot l_{act}(x, \alpha) \qquad i = 7 \text{ to } 9$$
(2)

- \$i\$ are the actuator velocities
- x is the position of the flap on the track: extended or retracted
- α is the rotational angle of the flap to the track: 0 to \pm 15° (retracted) & 25 to \pm 15° (extended)
- \propto is the flap rotational angle amplitude, 15° or $1/12\pi$ rad
- f is the frequency, 1 Hz to realize the desired flap rotation speed of 60°/s
- $I_{act}(x,\alpha)$ is the arm of the rotation actuator to the FWD flap lug, depending on x and α

Equation (2) is approximated by assuming an average arm of the rotation actuator to the FWD flap $l_{act\ nom}$:

$$\dot{s}_{i,max} = 0$$
 $i = 1 \text{ to } 6$
 $\dot{s}_{i,max} \approx 2 \cdot \pi \cdot f \cdot \infty \cdot l_{act_nom}$ $i = 7 \text{ to } 9$ (3)

Consequently the volumetric oil volume for each actuator can be determined by multiplication of (1) and (3):

$$Q_{i} = 0 i = 1 \text{ to } 6$$

$$Q_{i} \approx 2 \cdot \pi \cdot f \cdot \propto l_{act_nom} \cdot \frac{F_{i}}{p_{c}} i = 7 \text{ to } 9$$
(4)

The basis for the layout of valves, piping, manifolds and accumulators is defined by taking equations (1) and (4) for the requested pressure and flow at each actuator location. The outcome was integrated by hand rules to an overall layout, taking into account pressure losses in piping and manifolds, please refer to Figure 10.

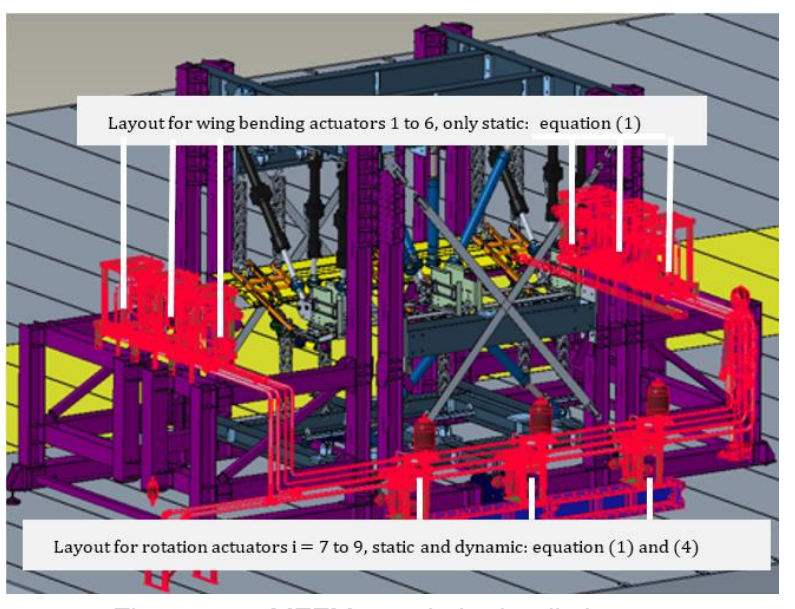


Figure 10 – MFFM test rig hydraulic layout.

3. Virtual test & MFFM Demonstration

Demonstration tests were successfully executed at the NLR test facility with the test set-up as described in section 2. The MFFM flap and supports were manufactured with representative stiffness and inertia properties, for which the ribs in the flap were topologically optimized, please refer to publications [4] and [5].

Figure 11 shows a momentum photo of the MFFM mechanism in the test rig during a dynamic test with the flap in retracted position at a rotational angle of approximately 10 degrees (trailing edge downwards).



Figure 11 – Photo of NLR test set-up.

During demonstrations, interface loads and strains on critical locations of the flap were real life correlated with predicted data to enable adjustment or stop of test execution in case of deviations. For this purpose a dedicated virtual test model was developed and coupled to the hydraulic control system. An additional future objective of the model is to explore and predict load and velocity limits of the test before to enable test set-up optimization in an early stage of the development process. The model is further developed in an NLR future aircraft wing demonstrator project using a Matlab Simulink model from which first results are expected in 2025.

The following sub sections provide a description of the virtual test model (section 3.1) as well as the outcome of demonstration testing with a correlation analysis between predicted data and test data (section 3.2).

3.1 Virtual test model

A virtual structural test model was developed providing test load and displacement predictions at discrete locations for each kinematic position of the flap. For this purpose a physical kinematic model of the MFFM flap and flap supports was coupled to a FEM of the flap and the test rig. The model is described in the most general form mathematically by equation (5), with a physical representation of the terms in Figure 12:

$$F_i = [K_{i,j}(x,\alpha)] \cdot [s_j,\alpha_j] + [C_{i,j}(x,\alpha)] \cdot [\dot{s}_j,\dot{\alpha}_j] + [M_{i,j}(x,\alpha)] \cdot [\ddot{s}_j,\ddot{\alpha}_j] + F_{i,0}$$

$$(5)$$

- F_i are the actuator loads on in the test set-up, i = 1 to 9
- $F_{i,0}$ are the actuator loads in neutral flap position
- x is the position of the flap on the track: extended or retracted
- α is the rotational angle of the flap to the track: 0 to \pm 15° (retracted) & 25 to \pm 15° (extended)
- $[K_{i,j}(x, \alpha)]$ is the integrated stiffness matrix, depending on the position x and rotational angle α
- $[C_{i,j}(x, \alpha)]$ is the integrated damping matrix, depending on the position x and rotational angle α
- $[M_{i,j}(x, \alpha)]$ is the integrated mass matrix, depending on the position x and rotational angle α
- $[s_i, \alpha_i]$ the linear and rotational displacement vector
- $[\dot{s}_i, \dot{\alpha}_i]$ the linear and rotational velocity vector
- $[\dot{s}_i, \ddot{\alpha}_i]$ the linear and rotational acceleration vector

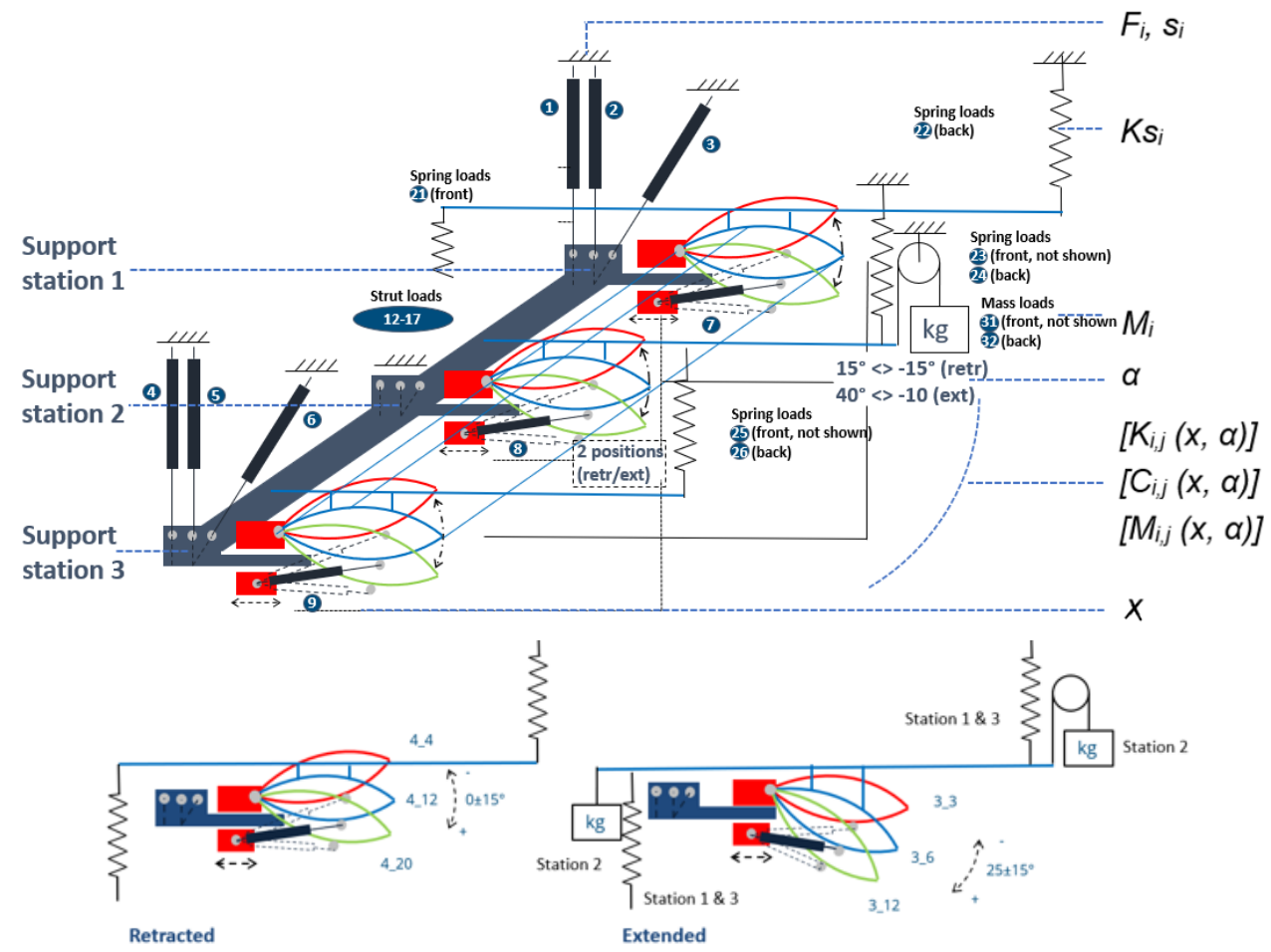


Figure 12 – 3D physical kinematic model (upper part) with 2D representations for the retracted (left) and extended (right) position (lower part).

During demonstration testing, wing bending is induced semi statically by load actuators 1 to 6 connected to the frame of the test rig, followed by dynamic flap rotation from the rotation actuators 7 to 9 with passive air loads induced by springs and masses. By consequently considering only static effects during wing bending and dynamic effects during flap rotation, equation (5) can be rewritten to equations (6a) for application of wing bending and (6b) for flap rotation under air load:

$$F_i = K_{i,j}(x,\alpha) \cdot s_j \qquad i, j = 1 \text{ to } 6$$
 (6a)

$$F_i = [Airload_i] \cdot l_s/l_{act} (x, \alpha)$$
 $i = 7 \text{ to } 9$ (6b)

$$= [Ks_i \cdot (\alpha \cdot l_s + e0_i) + M_i \cdot l_s \cdot \ddot{\alpha} + M_i \cdot g] \cdot l_s / l_{act} (x, \alpha)$$

- F_i are the actuator loads in the test set-up, i = 1 to 9
- $K_{i,j}(x,\alpha)$ is the integrated stiffness matrix, depending on the position x and rotational angle α
- s_i are the wing bending displacements in the actuators
- Airload_i is the combined FWD &AFT air load on a support
- Ks; are the combined FWD & AFT air load spring stiffnesses
- e0; are the spring elongations in neutral flap position
- Is is the arm of the spring to the FWD flap lug
- $I_{act}(x,\alpha)$ is the arm of the rotation actuator to the FWD flap lug, depending on x and α
- M_i are the air combined FWD & AFT load masses
- α is the rotational angle of the flap to the track: 0 to \pm 15° (retracted) & 25 to \pm 15° (extended)
- \ddot{a} is the rotational acceleration
- *g* is the gravitational constant representing the gravitational acceleration

The Stiffness matrix $K_{i,j}(x,\alpha)$ in (6a) to model the effects of wing bending is calculated by FEM analysis for discrete positions of x and α and this was repeated for the intact conditions as well as jamming and disconnect scenario's, resulting in a unique stiffness matrix for each situation. In theory the matrix can be determined for each intermediate situation with the help of an interpolation technique, however for demonstrations purposes the model was only applied for data correlation on the discrete positions.

The terms in (6b) to model the effects of flap rotation are related to the MFFM kinematic. These terms can be calculated analytically straightforward with a relation for the rotation actuator arm l_{act} (x, α) as function of x and α , where the spring stiffness's Ks_i are calibrated on measured data. The model does not take into account effects of structural damping and friction in the test setup yet, which can lead to deviations at load equilibrium calculations. The complete structural test model is illustrated by Figure 13, showing the combination of a physical model together with FEMs of the test rig and MFFM flap.

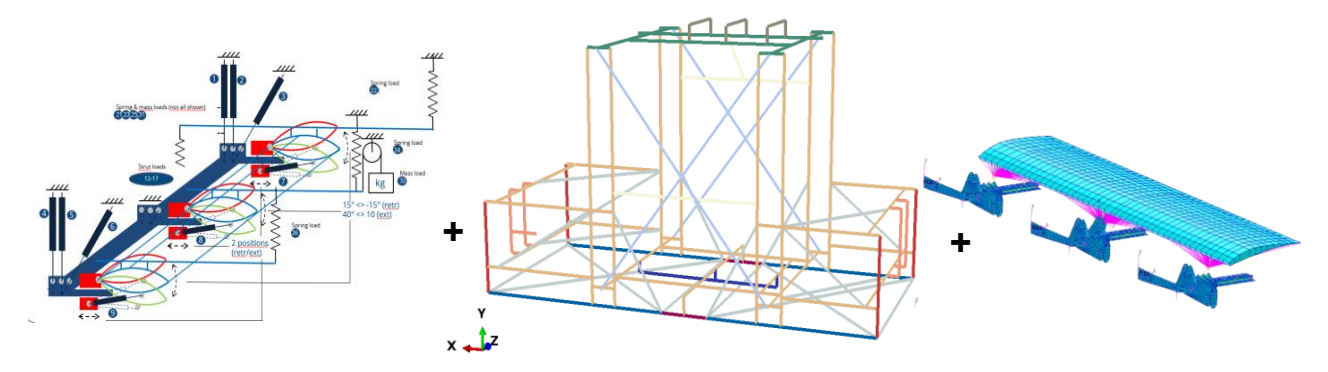


Figure 13 – Virtual test model: Physical model (left), Test rig FEM (mid) & MFFM FEM (right).

In the future the model will be extended with a hydraulic module to predict the dynamic response and optimize the test set-up before the final design & construction. Equations (7) provide the basic formula for a hydraulic actuation module:

$$F_i = pv_i \cdot Ac_i \tag{7a}$$

$$\dot{pv}_i = \left(\frac{u_i}{u_{max}} \sqrt{\frac{p_s - pv_i}{\Delta p_n}} \cdot Q_n - Ac_i \cdot \dot{s}_i\right) \frac{\beta}{V + Ac \cdot s_i}$$
(7b)

- F_i are the actuator loads in the test set-up
- s_i are the actuator displacements and s_i the actuator velocities
- pv_i is the hydraulic pressure in an actuator and pv_i the hydraulic pressure variation with the time
- Ac_i , u_i , u_{max} , p_s , Δp_n , Q_n , β , V are parameters of the actuator and hydraulic fluid

The hydraulic module can be coupled to the current model by considering equilibrium between equation (5) and (7a). This will be elaborated for the 2025 NLR aircraft wing demonstrator from which the first results are expected in the second half of 2024 and is out of scope for this paper.

3.2 Demonstration testing & correlation synthesis

Demonstration testing was executed firstly for the extended position and subsequently for the retracted position. In addition to correlation of measurements with predicted loads and displacements, strain gauge readings at critical locations on the MFFM flap lugs were monitored and compared with FEM predictions in order to adjust or stop the test in case of unexpected deformations, please refer to Figure 14.

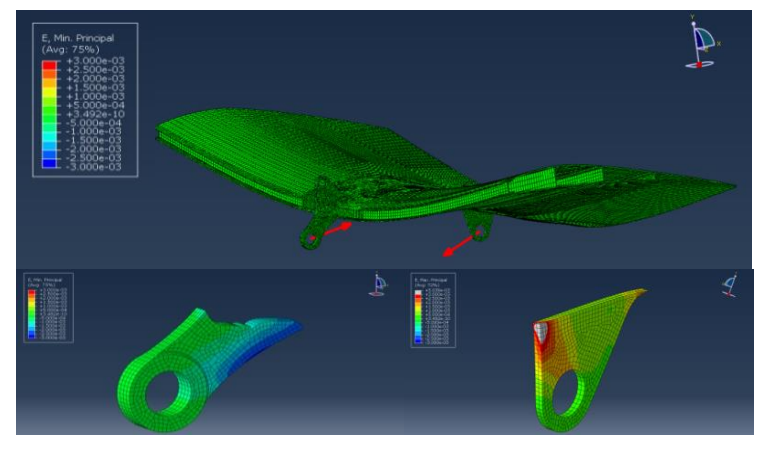


Figure 14 – Critical strains at forward and offset lugs (retracted position, rotation actuator 2 disconnect case).

To systematically build up the load levels, the tests were started by application of wing bending, please refer to the light grey area in Figure 15 to Figure 19. Subsequently the air load in neutral position (25° for the extended position and 0° for the retracted position) was applied by manually pretensioning the air load springs and application of masses, indicated by the dark grey area. Then the flap was semi statically rotated sinusoidal over a range of $\pm 15^{\circ}$ referred to by the green area. After successful static rotation, a dynamic test was executed with gradual increasing rotational velocity until the target of 60°/s flap speed was reached. After the test the air load and wing bending were released in the light blue area.

This procedure was executed for intact cases as well as for jamming and disconnect cases. In case of a jamming load case, carriage skew was actuated by manually pressurizing the translation actuators, please refer to the yellow area in Figure 18 and Figure 19. Figure 15 shows detailed correlation plots of air loads and actuator loads for the intact load case in retraced position of the flap. To exclude any variation due to inaccuracy with respect to spring specifications, the predictions are

rerun based and calibrated on measured spring pretension and stiffness. As a consequence, the left side shows a perfect fit. On the right side, during the wing bending phase the actuator loads increase from initial zero load to relative small compressive loads at support stations 1 and 3 and a small tension load in support 2. It is observed that predicted values differ slightly from measurements and the direction of load at support 3 is opposite compared to the prediction. During the aero load phase, the actuator load on support 1 resembles well the predictions, the actuator load on support 2 is larger as predicted and the load on support 3 smaller, which implies that the air load distribution is slightly different from predictions. During flap rotation the initial load distribution offset remains constant and the trend of measurements corresponds well with predictions.

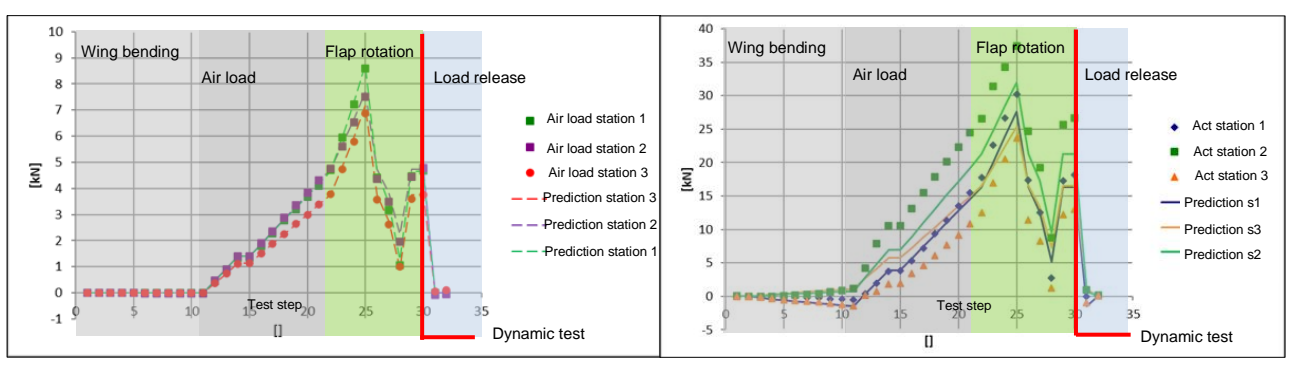
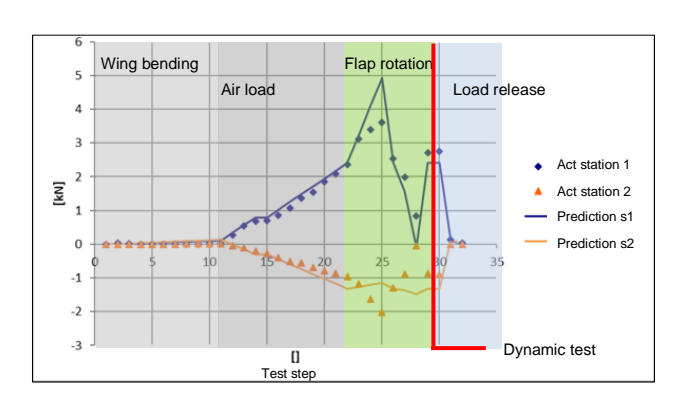


Figure 15 – Correlation air loads (left) & rotation actuator loads (right).

Figure 16 shows the loads in the translation actuator for the intact load case in retracted position of the flap. The measured loads follow well the predictions until the flap is rotated, where it can be observed that the loads at support station 1 develop slower as predicted and the loads on support 2 faster. This is probably caused by stiffness deviations of the manually controlled translation actuators which use less rigid tubing and larger oil volumes compared to aircraft technology.

Figure 17 provides a plot of the rotation actuator loads as function of the time during the dynamic phase of the test, merely illustrating that the targeted flap speed of 60° rotational speed is reached without deviations by a sinusoidal load and displacement trajectory.



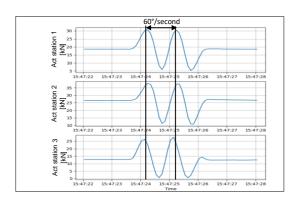


Figure 16 – Correlation translation actuator loads.

Figure 17 – Dynamic rotation actuator loads.

Figure 18 and Figure 19 provide correlation plots on induced air loads and rotational moment from the actuators loads for the most severe load cases of jamming of the carriage on support station 2. The air load results show a proper correlation between load measurements and predictions. It is expected that the rotational moment resulting from the actuator loads (*Mz_rotor_act*) are in equilibrium with the air load moments (*Mz_airload*), however the actuator loads show slightly higher readings with a maximum deviation of approximately 15%. Hypothesis is that geometrical non

linearity due to wing bending together with friction of the cable pulleys to transfer the air loads from springs and masses to the flap cause this deviation. This is supported by earlier findings on the effect of wing bending causing op to 5% deviation and the effect of pulley friction causing up to 10% depending on the use configuration (pulley angles and side loads). Note that due to the absence of friction and damping effects in the actual virtual test model these findings were not predicted either, so the model must be extended with friction and damping to predict and minimize these effects in the future. The same effect is probably accountable for the slight differences between predictions and measurements for air load and actuator loads at the intact load cases.

In addition to data correlation, dynamic analyses have been performed to predict the response of the flap on aircraft wing level. Those have shown that the behavior of the flap at high rotation speeds remains effective leading to a good performance of this control surface in all conditions.

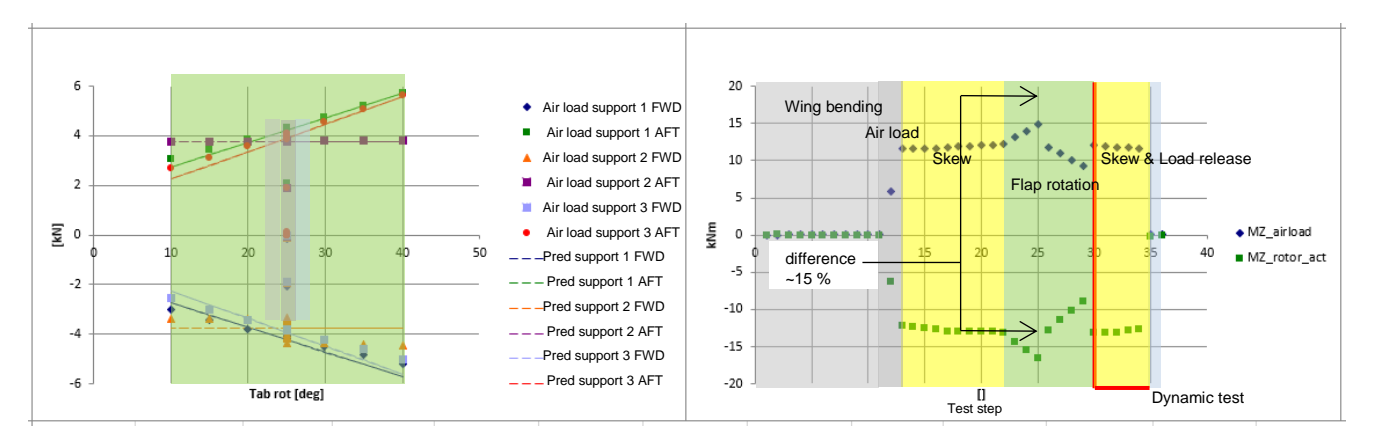


Figure 18 – Correlation air load and rotation moment extended position, carriage station 2 jammed.

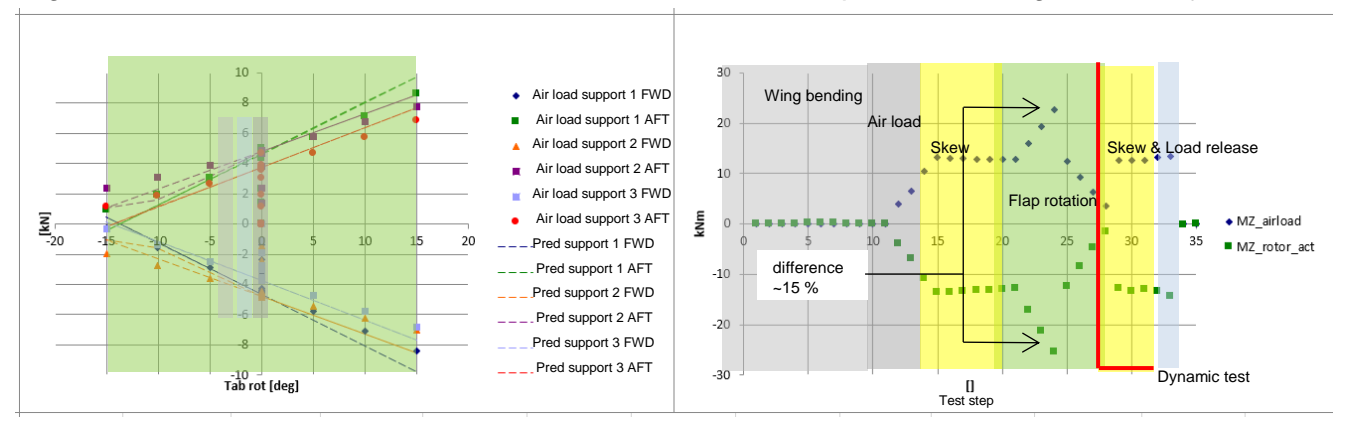


Figure 19 – Correlation air load and rotation moment retracted position, carriage station 2 jammed.

4. Flexible Tube test

4.1 Test set-up development

Objective of the flexible tube test is to demonstrate that the integrity of the tube remains unaffected due to cycling from the retracted to the extended position during the aircraft's operational life, please refer to Figure 20.

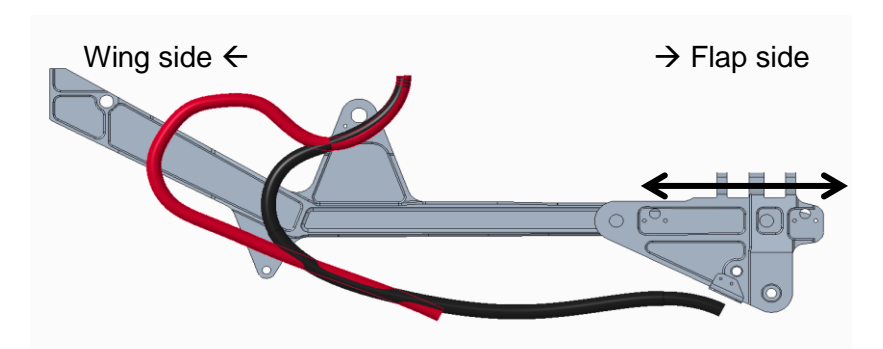


Figure 20 – Cyclic movement from retracted (red) to extended (black) position.

For this objective a statically determined dummy track structure is developed which is fixed in 6 degrees of freedom by beam connections (b1 to b6) on the wing side. The movement on flap side is realized with an hydraulic test actuator and the reaction forces on the flap side are measured with 3 load cells, please refer to Figure 21. Potential sideway bending and wear of the tube is monitored and recorded with a camera.

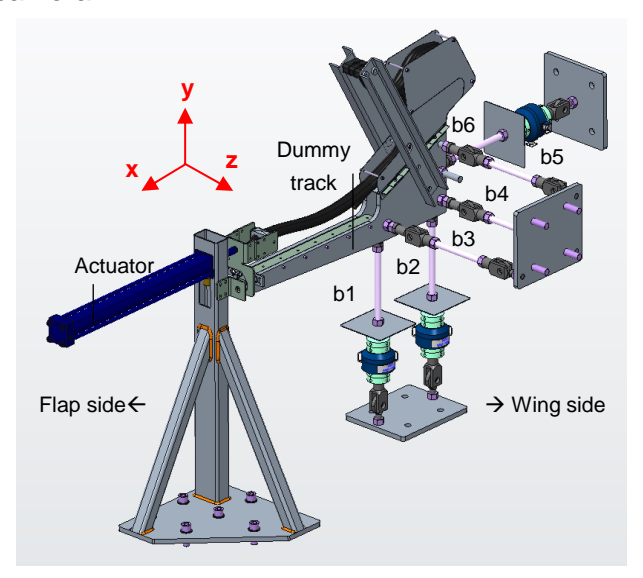


Figure 21 – Statically determined flexible tube test principle.

To simulate realistic environmental conditions, a climatic chamber is constructed around the test rig, which is also used to apply contaminants in a contained way, as illustrated in Figure 22.

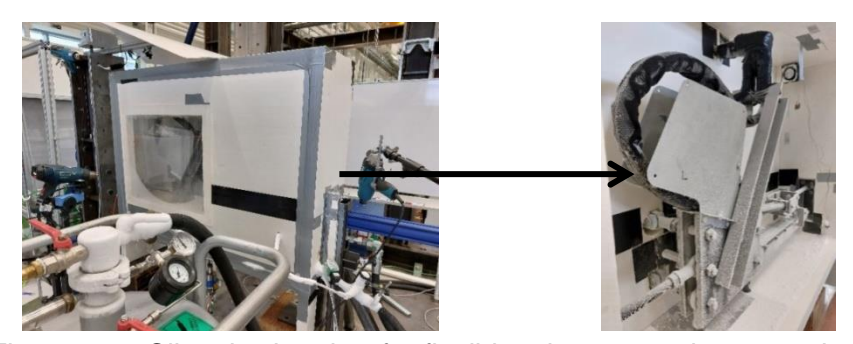


Figure 22 – Climatic chamber for flexible tube test environmental conditions.

4.2 Demonstration testing

Demonstration tests were successfully executed at the NLR test facility in 4 phases in with variable environmental conditions (room temperature, low temperature of -55°C, contaminants) and protection measures, please refer to Table 1.

Table 1— Test phase overview.				
	Phase 1	Phase 2	Phase 3	Phase 4
Temperature	Room temperature	Room temperature	-55°C ± 3°C	Room temperature
Tube pressure	350bar +/-5%	350bar +/-5%	350bar +/-5%	350bar +/-5%
Actuator speed	0.1m/s	0.1m/s	0.1m/s	0.1m/s
Cycle frequency	0.111Hz	0.111Hz	0.111Hz	0.111Hz
Number of cycles	100	27,000	6,000	27,000
Protection	Small bracket	Protection bracket	Protection bracket	Protection bracket
		Protection sleeve	Protection sleeve	Protection sleeve
Monitoring	2 cameras	2 cameras	2 cameras	2 cameras
	Pressure switch	Pressure switch	Pressure switch	Pressure switch
Data acquisition		3 load cells	3 load cells	3 load cells
		1 displacement transducer	1 displacement transducer	1 displacement transducer
		tube pressure	tube pressure	tube pressure
Contaminants				Skydrol, Jet Fuel A1
				Salt water 3.5%
				Sand 0.4-0.8mm

Table 1– Test phase overview.

Figure 23 shows the result for each phase after endurance testing. For all configurations no bending or excessive wear was observed, which means that the flexible tube will function reliably in aircraft conditions when integrated with the MFFM mechanism.









Figure 23 – Flexible tube test result for phase 1(left), 2 (mid-left), 3(mid-right) and 4(right).

5. Conclusions & Recommendations

The novel test rig to demonstrate the performance of an innovative new Multi-Functional Flap Mechanism (MFFM) has performed well for this kind of complex testing. However, demonstration tests have shown limitations on both the test article and the test rig.

Due to significant friction in the cable pulleys for load transfer from springs and masses to the flap to simulate air loading, the final applied load at flap level deviates from the intended load, which is observed by larger rotation actuator forces up to 15%. Hence an alternative load application or capturing method should be investigated to further improve testing with more realistic air loads in future.

To position the flap in extended or retracted position, manually controlled translation actuators have been applied. Due to a deviating stiffness of these actuators, load correlation with the predicted data is not optimal.

Further test rig improvements are the incorporation of more complex air loading possibilities. With the actual test rig, only the application of air loads with a resulting pure rotation moment on the flap, is possible. This is sufficient for demonstration purposes but should be expanded for certification goals.

An additional key element of the MFFM is the flexible tubing for hydraulic supply of the rotation actuators. A proper static determined test set-up was developed which has demonstrated that the tube is able to supply the necessary pressure to the moving actuator in different conditions (cold temperature, contamination) throughout the complete life of the aircraft.

A proper basis is developed for a virtual structural test model. Although the model requires further improvement by using a simulation program environment like Matlab-Simulink, the actual predictions are accurate and provide a good insight in the structural response. The model must be extended with a hydraulic module together with friction and damping effects to optimize dynamic response predictions.

6. Contact Author Email Address

mailto: <u>Jan.Docter@nlr.nl</u> mailto: <u>Hermen.Pijlman@nlr.nl</u>

mailto: <u>Dirk.DeWit@ ascoindustries.com</u> mailto: <u>Johan.Vervliet@ ascoindustries.com</u>

7. Copyright Statement

The authors confirm that they, and/or their company or organization, hold copyright on all of the original material included in this paper. The authors also confirm that they have obtained permission, from the copyright holder of any third party material included in this paper, to publish it as part of their paper. The authors confirm that they give permission, or have obtained permission from the copyright holder of this paper, for the publication and distribution of this paper as part of the ICAS proceedings or as individual off-prints from the proceedings.

References

- [1] https://www.nlr.nl
- [2] https://www.asco.be
- [3] https://www.clean-aviation.eu/clean-sky-2/programme-overview-and-structure/high-level-objectives
- [4] Desmet M. Cs2 manta multi-functional flap mechanism offering a second degree of freedom. 33rd Congress of the international council of the aeronautical sciences, Stockholm, 2023.
- [5] Montero-Sistiaga M L, Haagsma R and Osinga T. Development of a production approach to build a titanium flaperon rib by directed energy deposition. *Progress in additive manufacturing*, pp 61–66, 2023.